MLL1 directs gut-associated antibody responses to helminth and bacterial infections

Yan Zhang[a,b,1], Clarissa Chakma[a,b,1], Alana Kirn[a,b], Aidil Zaini[a,b,c], Rohia Farighi[a,b,c], Liang Xie[b,d,†], Diana López-Ureña[d,e], Steven Mileto[d,e], Dena Lyras[d,e], Colby Zaph[a,b], Joanna R Groom[f,g], and Kim L Good-Jacobson[a,b,*].

[a]Department of Biochemistry and Molecular Biology, Monash University, Clayton, Victoria, Australia 3800.

[b]Immunity Program, Biomedicine Discovery Institute, Monash University, Clayton, Victoria, Australia 3800.

[c]Department of Immunology, Alfred Medical Research and Education Precinct, Monash University, Melbourne, VIC, Australia.

[d]Department of Microbiology, Monash University, Clayton, Victoria, Australia 3800.

[e]Infection Program, Biomedicine Discovery Institute, Monash University, Clayton, Victoria, Australia 3800.

[f]Division of Immunology, Walter and Eliza Hall Institute of Medical Research, Parkville, Victoria, Australia.

[g]Department of Medical Biology, University of Melbourne, Parkville, Victoria, Australia.

†Present address: Precision Medicine Translational Research Programme, Department of Obstetrics & Gynaecology, Yong Loo Lin School of Medicine, National University of Singapore, Singapore.

[1]Equal contribution

*Correspondence: Kim Good-Jacobson

Email: kim.jacobson@monash.edu

Author contributions: KLG-J conceived the study; KLG-J and YZ designed research; YZ, CC, AK, AZ and RF performed research; KLG-J, CC, AK and YZ analyzed data; CZ, DL and JRG provided intellectual input; CZ, LX, DLU, SM and JRG provided reagents and technical expertise; and KLG-J, YZ and CC wrote the manuscript.

Competing Interest Statement: The authors declare no competing interests.

Keywords: B cells, IgA, helminth, trichuris muris, epigenetics, gut-associated lymphoid tissue, MLL1.

Abstract

Soil-transmitted helminths are one of the most common infections across the world, yet how to promote an effective humoral response to helminths is not well understood. To ensure the most effective response, molecular programs underpin the specialization of antibody effector subtype to microenvironmental signals. Here, we identify the methyltransferase mixed-lineage leukemia 1 (MLL1) as a key target to promote IgA-driven responses. *Mll1* was increased in germinal center (GC) B cells in gut-associated lymphoid tissues, and the absence of MLL1 in mature B cells led to significant reductions in GCs, IgG1 and IgE in response to the helminth *Trichuris muris*. Yet, worm expulsion occurred more rapidly in *Mll1*$^{f/f}$*Cd23*$^{cre/+}$ mice compared to control mice in the first two weeks of infection. Accelerated worm clearance correlated with significantly elevated IgA^{+} plasma cells (PC), serum IgA and fecal IgA in in *Mll1*$^{f/f}$*Cd23*$^{cre/+}$ mice. Stimulation of B cells *in vitro* confirmed that *Mll1*-deficiency accelerated the formation of IgA^{+} PC and that this effect was B cell-intrinsic. CCR9 was identified as a key MLL1-regulated molecule by RNA-sequencing and flow cytometry. Correspondingly, *Mll1*$^{f/f}$*Cd23*$^{cre/+}$ mice infected with either *T. muris* or the bacterium *C. rodentium* significant increased IgA^{+}CCR9^{+} PC localized in the large intestine. This tailoring of the B cell response to promote IgA-secreting PC correlated to a healthier microbiome in *Mll1*$^{f/f}$*Cd23*$^{cre/+}$ mice, compared to control mice. Thus, this study reveals MLL1 as a key target to tailor B cell responses to helminth infections, which may aid the development of effective mucosal vaccines or new targeted treatments.

Significance statement

Diseases caused by infections, such as soil-transmitted helminth infections or bacterial infections, continue to pose a major human health problem worldwide. One key reason why soil-transmitted

24 helminths continue to cause long-term health and economic burdens is the lack of an effective
25 vaccine for human use. Antibody responses underpin most successful vaccine designs. Therefore,
26 a comprehensive understanding of how B cell responses are regulated to produce tailored antibody
27 to different pathogens is critical for the development of effective therapeutics and vaccines. This
28 study uncovered MLL1 as a novel therapeutic target to promote IgA-producing plasma cells,
29 opening new avenues of investigation into how effective and tailored antibody responses may be
30 produced in response to bacterial or helminth infection.
31
32

Main Text

Introduction

Soil-transmitted helminth infections infect approximately one-quarter of the world's population, causing severe morbidity and death in high-incidence countries (1-5). Roundworm (*Ascaris lumbricoides*), whipworm (*Trichuris trichiura*) and hookworms (*Necator americanus and Ancylostoma duodenale*) are the most common soil-transmitted helminths that infect humans (6, 7). Currently, the most effective treatment for soil-transmitted helminth infections is to use mass anti-helminthic drug administrations, such as albendazole (8). However, long-term mass anti-helminthic drug therapy induces the development of drug-resistant parasites, and the treatment of reinfection causes a significant economic burden (9-11). Therefore, successful long-term public health interventions such as effective vaccines are urgently needed (12). B cell-mediated antibody responses are the basis of most successful vaccines, yet there is a lack of understanding of how to promote a potent humoral response to intestinal helminth infections.

Helminth-induced immune responses to whipworms such as *T. trichiura* mainly occur in the gut-associated lymphoid tissues (GALT) and are largely dominated by Th2-biased responses (13). Humoral responses in the GALT are highly specialized to maintain gut homeostasis by regulating commensal microbiota and responses to food antigens, pathogenic bacteria or helminths (14). The isotype of antibody produced during infection is critical for the effectiveness of the response (15). While IgG, IgE and IgA are all produced during mucosal responses (8), IgA is particularly crucial for the protection of the human intestinal mucosa (16-18). Increased IgA has been correlated to reduced helminthiasis, increased microbiota diversity and improved responses to pathogenic bacteria such as *Salmonella* Typhimurium (19-25).

56

57 Pinpointing key drivers of effective B cell responses in the GALT may aid development of effective
58 mucosal vaccines and new treatments for helminth infections. MLL1 (also known as KMT2A) is
59 a histone methyltransferase which promotes B cell development (26). It also can induce *Gata3*,
60 the master transcriptional factor for Th2 differentiation (27), and regulates Muc2 production by
61 intestinal stem cells, the major intestinal mucin that can provide protection against worms in the
62 colonic epithelium (28). Recent work has revealed that during immune responses, histone
63 modifiers have unique roles in regulating B cell subset formation, B cell migration, the quality and
64 quantity of antibody, and immunopathology (29-35). Given the role of MLL1 in promoting Th2
65 cells through cooperation with c-Myb (36), a transcription factor we have previously found to be
66 important in tailoring effective antibodies in response to a Th2-induced microenvironment (15),
67 we hypothesized that MLL1 could be a key regulator of B cell responses in the GALT. Here, we
68 find that conditional deletion of MLL1 in mature B cells promotes IgA responses to the helminth
69 infection *Trichuris muris*. *Mll1*$^{f/f}$*Cd23*$^{Cre/+}$ mice demonstrated accelerated worm clearance and
70 anti-inflammatory microbiota. Compared with control mice, *Mll1*$^{f/f}$*Cd23*$^{Cre/+}$ mice infected with
71 either *T. muris* or the bacteria *Citrobacter rodentium* had significantly increased IgA production
72 and IgA^{+}CCR9^{+} plasma cells (PC). These results identify a role for IgA in the protection against
73 *T. muris* infection and identify MLL1 as a therapeutic target to promote the production of IgA^{+}
74 PC.

75

Results

MLL1 is required for optimal GC B cell responses

To investigate whether MLL1 may tailor mucosal B cell responses, we first examined the expression of *Mll1* in mature B cell subsets in GALT. B cell subsets were sort-purified from naïve wild-type mice and assessed for *Mll1* expression by RT-qPCR in isolated mesenteric lymph nodes (mLN) and Peyer's patches. At steady-state, there is an active immune response to microbiota in the gut-draining secondary lymphoid organs, in which activated B cells can form extrafollicular antibody-secreting PC, or germinal centers (GC) (2, 37). GCs provide a site for affinity maturation of B cells, enabling the production of long-lived memory B cells and PC, two populations that can persist for long periods of time to provide immunity (38). In comparison to naïve B cells and PC, GC B cells had significantly increased expression of *Mll1* (Fig. 1A-B). To determine whether this increase in *Mll1* in GC B cells was observed systemically, we immunized wild-type mice with (4-hydroxy-3-nitrophenyl)acetyl conjugated to keyhole limpet hemocyanin (NP-KLH), a haptenated protein precipitated in the adjuvant alum, and assessed *Mll1* in sort-purified subsets post-immunization. Commensurate with GALT GCs, *Mll1* was significantly upregulated in splenic GC B cells compared to follicular B cells (Fig. 1C). A small but non-significant increase in *Mll1* expression was also detected in memory B cells, compared to follicular B cells (Fig. 1C).

Given the increased expression of *Mll1* in GC B cells, we assessed whether MLL1 was required for GC formation. To conditionally delete *Mll1* in B cells, we crossed *Mll1* floxed mice to mice in which *Cre* is under the control of the *Cd23* promoter. Thus, upon Cre expression, *Mll1* would be expressed normally during B cell development, but conditionally deleted within mature B cells. To assess Th2 responses, we used the *T. muris* model of human *T. trichuria* whipworm infection.

99 *T. muris* is antigenically similar to *T. trichuria*, and both elicit a similar type of immune response,
100 making *T. muris* an effective model to study the B cell response to intestinal helminth infection
101 (13, 39, 40). *Mll1*$^{f/f}$*Cd23*$^{cre/+}$ and *Cd23*$^{cre/+}$ controls were infected with *T. muris* and B cell responses
102 assessed over time (Fig. 1D). The frequency of GC B cells was significantly decreased in
103 *Mll1*$^{f/f}$*Cd23*$^{cre/+}$ mice compared to control mice at each time point post-infection. A 1.5-fold, 4.5-
104 fold and 1.7-fold reduction in the number of GC B cells was observed in B cell-specific MLL1-
105 deleted mice compared to control mice on days (d)14, d28 and d35, respectively (Fig. 1E-G).
106 Histological analyses confirmed that GC structures were less frequent in mLN in the absence of
107 *Mll1* (Fig. 1H).
108
109 To understand whether the role for MLL1 in GC biology was limited to GALT, or whether it was
110 generalizable to other types of B cell responses, *Mll1*$^{f/f}$*Cd23*$^{cre/+}$ and *Cd23*$^{cre/+}$ mice were
111 immunized with alum-precipitated NP-KLH and GC B cell formation assessed in the spleen (Fig.
112 I-K). Use of this model antigen allows the assessment of T-dependent B cell differentiation in the
113 absence of the pathogen-influenced changes to the tissue microenvironment that occurs upon
114 infection. In the absence of *Mll1*, GC B cells were virtually absent on d14 and d28 (Fig. I-K).
115 Therefore, MLL1 was required for effective GC B cell responses in response to infection or
116 immunization.
117
118 ***Mll1 deletion induces preferential production of IgA over IgG1 and IgE***
119 B cell responses are important for reducing worm burden (37, 40). Thus, given the reduction of
120 GC B cells, we hypothesized that there would be a reduced ability of MLL1-deficient mice to
121 expel worms. To our surprise, worm clearance occurred more rapidly in *Mll1*$^{f/f}$*Cd23*$^{cre/+}$ mice,

122 compared to *Cd23*$^{cre/+}$ controls, with a >3-fold reduction on d14 post-*T. muris* infection (Fig. 2A).
123 Thus, conditional deletion of *Mll1* within mature B cells led to a more efficient and accelerated
124 worm expulsion during the early stages of *T. muris* infection.
125
126 B cells and helminth-specific antibodies can contribute to relieving worm burden (40). IgG1 and
127 IgE isotypes were assessed on 14 days post-infection to investigate whether accelerated worm
128 expulsion in *Mll1*$^{f/f}$*Cd23*$^{Cre/+}$ mice correlated to a change in the subclass dominating the response.
129 *T. muris*-specific IgG1 was reduced significantly in the absence of functional MLL1 (Fig. 2B), as
130 was the frequency of IgG1^{+} or IgE^{+} GC B cells and IgG1^{+} or IgE^{+} PC (Fig. 2C-G). Thus, these
131 results implied that IgG1 and IgE were not responsible for the accelerated worm clearance
132 observed in *Mll1*-deficient mice.
133
134 IgA is also key in the protection of human and murine intestinal mucosa (16, 18). IgA antibodies
135 have been linked to *T. muris* worm expulsion from the intestine (25). Thus, we investigated
136 whether MLL1 regulates the production of IgA. As mLN and Peyer's patches are both IgA-
137 inductive sites in the intestinal system (41), IgA^{+} cells were studied in both sites on d14 post-
138 infection. Both mLN and Peyer's patches showed increased IgA^{+} GC after B cell-intrinsic deletion
139 of *Mll1* (Fig. 2H-J). Accordingly, serum total IgA (Fig. 2K) and fecal total IgA (Fig. 2L) were both
140 significantly increased in *T. muris*-infected *Mll1*$^{f/f}$*Cd23*$^{Cre/+}$ mice compared to control mice. It was
141 possible that this increase in IgA may already have been present in *Mll1*$^{f/f}$*Cd23*$^{Cre/+}$ mice prior to
142 infection, and not directly driven by the B cell response to *T. muris* infection. We therefore assessed
143 IgA levels in uninfected mice. Fecal total IgA (Fig. S1A) and serum total IgA (Fig. S1B) were
144 comparable between uninfected *Cd23*$^{cre/+}$ and *Mll1*$^{f/f}$*Cd23*$^{Cre/+}$ mice, indicating that the elevated

145 IgA detected in the absence of *Mll1* was specifically induced by *T. muris* infection. Thus, while
146 IgG1$^+$ and IgE$^+$ cells were decreased in the absence of MLL1 *in vivo*, IgA was significantly
147 increased, correlating with accelerated helminth expulsion.
148
149 To examine whether the increased production of IgA observed *in vivo* was due to B cell-intrinsic
150 or B cell-extrinsic mechanisms, we assessed the ability of MLL1-deficient B cells to differentiate
151 into IgA$^+$ PC *in vitro*. Naïve B cells from *Mll1*$^{f/f}$*Cd23*$^{cre/+}$ and *Cd23*$^{cre/+}$ mice were stimulated *in*
152 *vitro* with IgA-promoting stimuli (CD40L, IL-4, IL-5, TGFβ and retinoic acid). After 4 days,
153 plasmablasts were assessed. MLL1-deficient cells had a significantly increased propensity to form
154 IgA$^+$ plasmablasts, compared to control B cells (Fig. 2M-O). This was also reflected in the increase
155 in IgA secreted in the cultures (Fig. 2P). Therefore, in the absence of MLL1, B cells were
156 intrinsically prone to produce IgA-producing PC.
157
158 ***MLL1 regulates intestinal localization of IgA$^+$CCR9$^+$ PCs***
159 We next investigated the transcriptional programs altered in the absence of MLL1 that may tailor
160 B cell responses in GALT. GC B cells (CD19$^+$IgD^{lo}CD95^{hi}CD38^{lo}) were sort-purified from mLN
161 of *T. muris*-infected *Cd23*$^{cre/+}$ and *Mll1*$^{f/f}$*Cd23*$^{cre/+}$ mice and RNA-sequencing undertaken. 33 genes
162 with > 2-fold expression change were observed in GC B cells after B cell-intrinsic deletion,
163 including 7 down-regulated genes and 26 up-regulated genes (Fig. 3A). Differential gene KEGG
164 enrichment analysis was performed to get further insight into the gene pathway in GC B cells
165 mediated by conditional deletion of *Mll1* in B cells. Consistent with the increased IgA in MLL1-
166 deficient mice, KEGG analysis identified a gene signature related to 'an intestinal immune network
167 for IgA production', along with several disease and stress pathways (Fig. 3B). Specifically, this

168 analysis identified *Ccr9* as significantly upregulated in *Mll1*$^{f/f}$*Cd23*$^{cre/+}$ mice than *Cd23*$^{cre/+}$ mice
169 (Fig. 3C).
170
171 Upregulation of CCR9 induces the migration of IgA^{+} PCs from mLN to the intestinal lamina
172 propria in response to CCL25 (42). Given that *Ccr9* was identified as differentially expressed in
173 the absence of *Mll1*, we examined whether MLL1 regulated CCR9 expression on IgA^{+} PCs in
174 GALT. In contrast to GC B cells (Fig. 3A-C), the frequency of CCR9^{+} IgA^{+} PCs and CCR9
175 expression on IgA^{+} PCs in mLN were decreased in MLL1-deficient mice (Fig. 3D-E), whereas
176 there was no change detected in the small intestine (data not shown). As *T. muris* infection mainly
177 occurs in the large intestine, including colon (43), we hypothesized that CCR9 may be regulating
178 IgA^{+} PC migration to the colon lamina propria (Fig. 3F). Indeed, the frequency of CCR9^{+} IgA^{+}
179 PCs was significantly increased in colon lamina propria of *Mll1*$^{f/f}$*Cd23*$^{cre/+}$ mice compared to
180 *Cd23*$^{cre/+}$ mice, respectively (Fig. 3G). Thus, these results indicated that B cell-specific *Mll1*
181 deletion increased CCR9^{+}IgA^{+} PCs to the colon.
182
183 To confirm that the observed regulation of IgA^{+} PC by MLL1 was not unique to the *T. muris*-
184 induced GALT immune response, we used the bacteria *Citrobacter rodentium*, which also induces
185 IgA production (44). *Mll1*$^{f/f}$*Cd23*$^{cre/+}$ and *Cd23*$^{cre/+}$ mice were infected with *C. rodentium* and
186 responses assessed at d14 post-infection (Fig. 3H). In accordance with the humoral response to *T.*
187 *muris*, *Mll1*-deficiency resulted in a significant decrease of CCR9^{+}IgA^{+} PC in mLN, coupled with
188 an increase of CCR9^{+}IgA^{+} cells in the colon lamina propria, and a concordant increase in serum
189 IgA (Fig. 3I-K). Taken together, the absence of *Mll1* in B cells leads to increased production of
190 IgA^{+} PC *in vitro*, as well as increased IgA and localization of CCR9^{+} IgA^{+} PCs in the colon lamina

191 propria in response to *T. muris* or *C. rodentium in vivo*.

192

193 ***B cell-intrinsic deletion of MLL1 induces changes to cecum morphology and microbiota***

194 Another key role for B cells and IgA in the GALT is the regulation of the microbiome (45, 46).
195 Helminth infection also has a significant effect on microbiota diversity, and in turn, the microbiota
196 can either support or help expel the helminth (47, 48). Given this, we hypothesized that the changes
197 to the humoral response and worm clearance in the absence of B cell expression of MLL1 may
198 lead to significant changes in the gut microenvironment and microbiota. To investigate, we tested
199 whether there were detectable changes to cecum morphology and microbiota diversity in
200 *Mll1*$^{f/f}$*Cd23*$^{cre/+}$ mice. Goblet cells secrete mucin, which can induce worm expulsion (49). A
201 significantly increased number of goblet cells was detected in the cecum of *T. muris*-infected
202 *Mll1*$^{f/f}$*Cd23*$^{cre/+}$ mice compared to *Cd23*$^{cre/+}$ mice on d14 post-infection (Fig. 4A, B). To investigate
203 microbiota diversity, 16S rRNA microbiome sequencing was performed on the cecal feces
204 collected 14 days post-*T.muris* infection (Fig. 4C; Fig. S1C-D). Although β-diversity did not show
205 a significant change (*p=0.0577*) (Fig. S1C), Linear discriminant analysis Effect Size (LEfSe)
206 identified significant changes in composition at genus level, with 5 bacterial groups positively
207 associated with *Mll1*$^{f/f}$*Cd23*$^{cre/+}$ mice compared to *Cd23*$^{cre/+}$ mice, and 4 genera found only in
208 *Cd23*$^{cre/+}$ mice (Fig. 4D, E). Functionally, bacteria with increased abundance have been noted as
209 beneficial, while decreased bacteria can be pathogenic (50-53). For example, the anti-
210 inflammatory bacteria *Prevotellaceae* and *Lachnospiraceae* (54, 55) are increased in
211 *Mll1*$^{f/f}$*Cd23*$^{cre/+}$ mice, with *Lachnospiraceae* negatively associated with *T. trichiura* egg burden
212 (51, 56). In contrast, microbiota that have been positively associated with helminth infection –
213 *Rikenellaceae* (48) and *Alloprevotella* (57) – were absent in in *Mll1*$^{f/f}$*Cd23*$^{cre/+}$ mice, compared to

214 *Cd23*$^{cre/+}$ mice (Fig. 4E). Taken together, B cell-intrinsic deletion of MLL1 altered the cecal
215 microbiota, correlating to a shift to a healthier microbiome during an IgA-dominated response to
216 helminth infection.
217

218 **Discussion**

219 Uncovering key regulators of mucosal immune responses is important for designing vaccines that
220 can induce effective protective responses harnessing the GALT. Here, we revealed the regulatory
221 role of MLL1 in worm clearance and the microbiota during helminth infection. MLL1 deletion in
222 mature B cells led to decreased GC B cells but increased IgA, correlating with accelerated worm
223 clearance and a decrease in pathogenic microbiota. Our study thus reveals a novel role for MLL1
224 in tailoring the antibody response, increases understanding of molecular regulators of humoral
225 response within the GALT, and provides a fundamental groundwork for developing therapeutics
226 to prevent or treat helminth infection.

227

228 During an immune response, B cell differentiation is orchestrated by both extrinsic and intrinsic
229 factors. The infecting pathogen or immunizing agent induces the activation of immune cells that
230 will secrete cytokines and other factors into the microenvironment, creating a milieu that will
231 influence the fate of B cells and type of antibody produced (38). These signals can then induce the
232 function of transcription factors and epigenetic regulators within the nucleus, to promote or repress
233 gene expression programs and ultimately, regulate B cell differentiation and function (58, 59).
234 While some key inducers of IgA isotype switching have been discovered, such as RUNX3 and
235 p300, TGFβ and retinoic acid (60-62), we reveal here that inhibiting MLL1 can significantly
236 increase production of IgA^+ PC, both *in vitro* and *in vivo*, and promotes the localisation of
237 $CCR9^+IgA^+$ cells in the colon lamina propria. There appeared to be a humoral response trade-off,
238 however, as GC B cells were significantly reduced and showed diminished frequencies of $IgG1^+$
239 and IgE^+ cells. These findings also point to non-overlapping roles of MLL1 and KMT2D (MLL2)
240 in B cell biology, as *Kmt2d* deletion promotes GC B cell formation (31). Unique roles for these

241 methyltransferases have also been noted in other systems, and is likely due to differing histone-
242 modifying activity and gene targets (63-65). In contrast to KMT2D, we did not observe global
243 H3K4me3 loss (data not shown). MLL1 has a wider array of histone-modifying activity and
244 molecular partners, and thus future studies should delineate the exact histone modifications and
245 target loci that are modified by MLL1 in GALT B cells.
246
247 Transmissible helminth infection affects approximately one quarter of the world's population (1-
248 5). Long-term drug therapy induces the development of drug-resistant parasites, and the treatment
249 of reinfection causes a huge economic burden (9). Therefore, successful long-term public health
250 interventions such as preventative vaccines are needed, but generation of an effective vaccine has
251 remained elusive. Furthermore, the need for promoting protective IgA through new-generation
252 mucosal vaccines extends beyond helminth-specific vaccines (66), and is an area of intense current
253 research. One major hurdle to the development of helminth-specific vaccines has been vaccine-
254 induced formation of antigen-specific IgE, leading to an allergic response (8, 12). In this context,
255 targeting MLL1 in B cells could provide benefit by repressing IgE while promoting IgA. Small
256 molecule inhibitors of MLL1 are in development for treatment of MLL-rearranged acute
257 leukemias (67). It is important to note that the delivery of a MLL1 inhibitor would need to be B
258 cell-targeted, given the roles of MLL1 in intestinal stem cells (28) and Th2 cells (27).
259
260 In summary, our study has uncovered MLL1 as a novel regulator of GALT B cell responses.
261 These results provide further understanding of the roles of histone modifiers in tailoring humoral
262 immune responses. More broadly, improving our understanding on how to promote effective

263 IgA-mediated responses in GALT will offer new avenues for oral and mucosal vaccine design

264 and in the treatment of intestinal helminth infection.

265

266 **Materials and Methods:**

267 **Mice**

268 *Cd23*$^{cre/+}$ mice (68) and *Mll1*$^{f/f}$ mice (69) were generously provided by Meinrad Busslinger
269 (Institute of Molecular Pathology, Austria) and Patricia Ernst (University of Colorado, USA),
270 respectively. *Mll1*$^{f/f}$*Cd23*$^{cre/+}$ on C57Bl/6 background were generated by crossing *Cd23*$^{cre/+}$ with
271 *Mll1*$^{f/f}$ mice. Mice were bred at the Monash Animal Research Platform under specific-pathogen-
272 free conditions. All animal experimentation was performed following the Australian National
273 Health and Medical Research Council (NHMRC) Code for the Care and Use of Animals for
274 Scientific Purposes. Procedures were approved by Monash and WEHI Animal Ethics Committees.
275 Both males and females, over 6 weeks old, were used in this study.

276

277 *Immunization:* Mice were intraperitoneally immunized with 100µg NP_{13}-KLH precipitated in the
278 adjuvant alum. *T. muris infection:* mice were infected with 200 *T. muris* eggs (70) by oral gavage.
279 *C. rodentium infection:* mice infected with $2x10^9$ colony-forming units of *C. rodentium* by oral
280 gavage.

281

282 **Flow cytometry, cell sorting and antibodies**

283 Single-cell suspensions were stained with fluorochrome-labelled antibodies (Table 1) in PBS
284 2%FCS for flow cytometric analysis or cell sorting as previously described (35). Rat IgG2b kappa
285 (2.4G2) was used to block the binding of antibodies by cell-surface Fc-receptors and normal rat
286 serum was used to block non-specific binding. For IgA staining, a transcription factor buffer set
287 (BD Pharmingen) was used following the manufacturer's recommendations. Cells were analyzed
288 using a BD-LSRFortessa X-20 flow cytometer and FACSDiva software (BD Biosciences). Data

289 was analyzed using FlowJo™ software (BD Life Sciences). For cell sorting, cells were sort-
290 purified using a BD Influx cell sorter (BD Biosciences).
291
292 **RT-qPCR**
293 Either RNeasy Plus Micro Kit (QIAGEN) or Direct-zol RNA Microprep kit (Zymo) were used to
294 extract RNA from sort-purified cells following the manufacturer's recommendations, and TRIzol
295 was used to extract RNA from homogenized proximal colon tissue. Reverse Transcription was
296 performed using High-Capacity cDNA Reverse Transcription kit (Thermo Fisher Scientific).
297 SYBR Green PCR kit (QIAGEN) was used to perform qPCR. *Rpl32* was used as an internal control
298 for normalization and calculating the ΔΔCt value (71). Primers used were: *Mll1* 5′-
299 GCAGATTGTAAGACGGCGAG-3′, 5′-GCAGATTGTAAGACGGCGAG-3′; *Rpl32* 5′-
300 ATCAGGCACCAGTCAGACCGAT-3′, 5′- GTTGCTCCCATAACCGATGTTGG-3′.
301
302 **Worm counting**
303 To determine worm clearance, ceca were collected from *T. muris*-infected mice, worms extracted
304 and counted.
305
306 ***T. muris*-specific ELISA**
307 High-binding 96-well ELISA-plates (Sarstedt) were coated with *T. muris* antigen (70) diluted in
308 carbonate buffer, and incubated overnight at 4°C. Following wash and blocking steps, samples that
309 were serially diluted and incubated for 1 hour at room temperature. After washing, anti-IgG1-HRP
310 (Southern Biotech) was added and incubated for 45 minutes at room temperature. The wells were
311 washed and TMB substrate (eBioscience) added, and after 1 minute, stopped with 1N HCl. Plates

312 were read at 450nm using a BMG OPTIMA plate reader.

313

314 **Serum IgA ELISA and fecal IgA ELISA**

315 *Sera:* blood was collected by cardiac puncture immediately post-mortem and sera collected post-
316 centrifugation. *Fecal extraction:* performed as previously described (72, 73) by adding 0.1g of
317 fecal pellets to 1ml of PBS containing complete mini protease inhibitor cocktail (Roche). Solids
318 were separated by centrifugation and supernatants (fecal extract) stored at -20°C until use. *IgA*
319 *ELISAs*: high-binding 96-well ELISA plates were coated using unlabelled IgA coating antibodies
320 (Southern Biotech). Following wash and blocking steps, samples that were serially diluted and
321 incubated for 37°C for 3 hours. Following washing, anti-IgA-HRP (Southern Biotech) was added
322 and incubated for 1 hour at 37°C. Plates were washed and developed with OPD-substrate solution
323 (Sigma-Aldrich). The plates were read at 450nm using a BMG OPTIMA plate reader.

324

325 **Immunohistochemistry**

326 mLN from *T. muris*-infected mice were first fixed in periodate-lysine-paraformaldehyde fixative,
327 immersed in 30% sucrose and then subsequently embedded and frozen in Optimal Cutting
328 Temperature compound (Tissue-Tek). 7µm tissue sections were cut using a microtome (Leica) and
329 mounted on Superfrost Plus slides (Thermo Fisher). Sections were fixed with cold acetone (Sigma)
330 at -20°C for 10 minutes. Sections were stained with PNA (Vector Labs) and B220 (BD Bioscience).
331 Slides were observed and images were captured under 4X and 10X magnification using a Nikon
332 microscope.

333

334 *Goblet cell immunohistochemistry*: formalin-fixed (10% neutral buffered), Swiss-rolled ceca were

335 stained with periodic acid Schiff and Alcian blue. Sections were scanned using an Aperio
336 Scanscope AT Turbo (Leica), at 20X magnification. Goblet cell number per crypt was counted for
337 20 crypts/mouse across the entire cecum using Aperio ImageScope (Leica) and ImageJ (NIH).
338

339 ***In vitro* B cell culture**

340 B cells from the spleen were isolated using the EasySep™ Mouse B Cell Isolation Kit
341 (STEMCELL Technologies) and labeled with Cell Trace Violet (ThermoFisher). $5x10^4$ labeled
342 cells were resuspended in B cell media (RPMI, 5%FCS, 50μM 2-mercaptoethanol and 2mM
343 glutamine) and stimulated with 50ng/ml CD40L (R&D Systems), 50ng/ml IL-4 (STEMCELL
344 Technologies), 5ng/ml IL-5 (R&D Systems), 10ng/ml TGFβ (R&D Systems) and 10nM retinoic
345 acid.
346

347 **RNA-sequencing**

348 GC B cells ($B220^+IgD^{lo}CD95^{hi}CD38^{lo}$) were sort-purified from mLN of *T.muris*-infected $Cd23^{cre/+}$
349 and $Mll1^{f/f}Cd23^{cre/+}$ mice. RNA was extracted using the RNeasy Plus Micro Kit according to the
350 manufacturer's instructions. Total mRNA was quantified with the Qubit Fluorometer (Invitrogen)
351 and RNA integrity number values were assessed using the Agilent Bioanalyzer. mRNA libraries
352 were sequenced on an Illumina Novaseq using a 2x150 paired-end (PE) configuration according
353 to the manufacturer's instructions. Data was processed and analysed as previously described (33,
354 35). The following values were used to detect differentially expressed genes: fold change >2; q-
355 value (FDR-adjusted p-value) < 0.05. KEGG (Kyoto Encyclopedia of Genes and Genomes)
356 enrichment analysis was performed using KEGG databases. Data has been deposited at GEO and
357 publicly available. Accession number is GSE237391.

358

359 **16S rRNA microbiome sequencing**

360 Feces from individual mice were collected from the cecum. DNA was extracted using ISOLATE
361 II Fecal DNA Kit (Bioline) according to the manufacturer's instructions. Amplicons were
362 generated from the V3 and V4 regions of 16S rRNA using 341F-targeted primers (5′-
363 CCTAYGGGRBGCASCAG -3′ and 5′-GGACTACNNGGGTATCTAAT-3′). Diversity profiling
364 analysis were performed with QIIME 2 2019.7 (74). Demultiplexed raw reads were primer
365 trimmed and quality filtered using the cutadapt plugin followed by denoising with DADA2 (75)
366 (via q2-dada2). Taxonomy was assigned to ASVs using the q2-feature-classifier (76) classify-
367 sklearn naïve Bayes taxonomy classifier. Linear Discriminant Analysis Effect Size (LefSe) was
368 performed using MicrobiomeAnalyst (77).

369

370 **Statistical analysis**

371 Experimental data are presented as mean ± standard error of the mean (SEM). Statistical analyses
372 performed with Mann-Whitney non-parametric test using GraphPad Prism 8 (GraphPad Software).
373 *$p < 0.05$, **$p < 0.01$ and ***$p < 0.001$. Mice assessed to be non-responders were excluded from
374 all analyses.

375

376 **Table 1. Antibodies**

Antibody	Fluorochrome	Company
CD19	APC-Cy7	Biolegend #B207588
CD95	PE-Cy7	BD Bioscience #7018663
CD38	Pacific Blue	Biolegend #B240225

IgD	A488	Biolegend #B206502
IgG1	APC	BD Bioscience #7128657
B220	PacBlue	Biolegend #B207505
IgM	PE	Biolegend #B221864
IgD	PerCp-Cy5.5	Biolegend #B186570
CD23	AF488	Biolegend #B156559
CD21/CD35	APC	Biolegend #B195498
CD5	Biotin	BD Bioscience #550874
CD3e	APC-Cy7	BD Bioscience #558117
CD19	PE	BioLegend #B207501
CD138	PE	BioLegend #B203320
IgE	FITC	BD Bioscience #5163873

377

Acknowledgements

We thank Moshe Olshansky, Alana Kirn and members of the Good-Jacobson lab for technical assistance; Patricia Ernst for *Mll* floxed mice, and staff of the Monash University FlowCore, Monash Animal Research Platform, Monash Histology Platform, and the Monash Genomics and Bioinformatics Platform. **Funding:** This work was supported by a Bellberry-Viertel Senior Medical Research Fellowship (KLG-J); National Health and Medical Research Council (NHMRC) Career Development Fellowship 1108066 (KLG-J); Australian Research Council (ARC) DP220102867 (KLG-J); Monash University-China Scholarship Council Joint PhD Scholarship (YZ); and Monash University Scholarships (CC, AZ, AK, LX).

389 **References**

390 1. P. M. Jourdan, P. H. L. Lamberton, A. Fenwick, D. G. Addiss, Soil-transmitted helminth
391 infections. *Lancet* **391**, 252-265 (2018).

392 2. A. Zaini, K. L. Good-Jacobson, C. Zaph, Context-dependent roles of B cells during
393 intestinal helminth infection. *PLoS Negl Trop Dis* **15**, e0009340 (2021).

394 3. WHO, Soil-transmitted helminth infections. *[online]* *https://www.who.int/news-*
395 *room/fact-sheets/detail/soil-transmitted-helminth-infections* (Accessed 2 March 2020).

396 4. D. W. Crompton, M. C. Nesheim, Nutritional impact of intestinal helminthiasis during the
397 human life cycle. *Annu Rev Nutr* **22**, 35-59 (2002).

398 5. L. Chelkeba, Z. Mekonnen, Y. Alemu, D. Emana, Epidemiology of intestinal parasitic
399 infections in preschool and school-aged Ethiopian children: a systematic review and
400 meta-analysis. *BMC Public Health* **20**, 117 (2020).

401 6. R. L. Pullan, J. L. Smith, R. Jasrasaria, S. J. Brooker, Global numbers of infection and
402 disease burden of soil transmitted helminth infections in 2010. *Parasit Vectors* **7**, 37
403 (2014).

404 7. J. C. Dunn, H. C. Turner, A. Tun, R. M. Anderson, Epidemiological surveys of, and
405 research on, soil-transmitted helminths in Southeast Asia: a systematic review. *Parasit*
406 *Vectors* **9**, 31 (2016).

407 8. A. Zawawi, K. J. Else, Soil-Transmitted Helminth Vaccines: Are We Getting Closer?
408 *Frontiers in immunology* **11** (2020).

409 9. C. E. James, A. L. Hudson, M. W. Davey, Drug resistance mechanisms in helminths: is it
410 survival of the fittest? *Trends Parasitol* **25**, 328-335 (2009).

411 10. J. C. Dunn *et al.*, Soil-transmitted helminth reinfection four and six months after mass
412 drug administration: results from the delta region of Myanmar. *PLoS Negl Trop Dis* **13**,
413 e0006591 (2019).
414 11. H. Dixon, C. E. Johnston, K. J. Else, Antigen selection for future anti-Trichuris vaccines:
415 a comparison of cytokine and antibody responses to larval and adult antigen in a primary
416 infection. *Parasite Immunol* **30**, 454-461 (2008).
417 12. D. J. Diemert, M. E. Bottazzi, J. Plieskatt, P. J. Hotez, J. M. Bethony, Lessons along the
418 Critical Path: Developing Vaccines against Human Helminths. *Trends Parasitol* **34**, 747-
419 758 (2018).
420 13. R. K. Grencis, Cytokine-mediated regulation of intestinal helminth infections: the
421 Trichuris muris model. *Ann Trop Med Parasitol* **87**, 643-647 (1993).
422 14. M. Bemark, M. J. Pitcher, C. Dionisi, J. Spencer, Gut-associated lymphoid tissue: a
423 microbiota-driven hub of B cell immunity. *Trends Immunol* **45**, 211-223 (2024).
424 15. D. Piovesan *et al.*, c-Myb Regulates the T-Bet-Dependent Differentiation Program in B
425 Cells to Coordinate Antibody Responses. *Cell Rep* **19**, 461-470 (2017).
426 16. J. Spencer, L. M. Sollid, The human intestinal B-cell response. *Mucosal Immunology* **9**,
427 1113-1124 (2016).
428 17. P. E. Conrey *et al.*, IgA deficiency destabilizes homeostasis toward intestinal microbes
429 and increases systemic immune dysregulation. *Sci Immunol* **8**, eade2335 (2023).
430 18. O. Pabst, New concepts in the generation and functions of IgA. *Nat Rev Immunol* **12**,
431 821-832 (2012).
432 19. A. C. S. Ramos *et al.*, The role of IgA in gastrointestinal helminthiasis: A systematic
433 review. *Immunol Lett* **249**, 12-22 (2022).

434 20. F. Fransen *et al.*, BALB/c and C57BL/6 Mice Differ in Polyreactive IgA Abundance,
435 which Impacts the Generation of Antigen-Specific IgA and Microbiota Diversity.
436 *Immunity* **43**, 527-540 (2015).
437 21. K. Koyama, H. Tamauchi, M. Tomita, T. Kitajima, Y. Ito, B-cell activation in the
438 mesenteric lymph nodes of resistant BALB/c mice infected with the murine nematode
439 parasite Trichuris muris. *Parasitol Res* **85**, 194-199 (1999).
440 22. M. Clerc, G. Devevey, A. Fenton, A. B. Pedersen, Antibodies and coinfection drive
441 variation in nematode burdens in wild mice. *Int J Parasitol* **48**, 785-792 (2018).
442 23. C. McGuire, W. C. Chan, D. Wakelin, Nasal immunization with homogenate and peptide
443 antigens induces protective immunity against Trichinella spiralis. *Infect Immun* **70**, 7149-
444 7152 (2002).
445 24. Y. Yang *et al.*, Oral vaccination with Ts87 DNA vaccine delivered by attenuated
446 Salmonella typhimurium elicits a protective immune response against Trichinella spiralis
447 larval challenge. *Vaccine* **28**, 2735-2742 (2010).
448 25. T. I. Roach, K. J. Else, D. Wakelin, D. J. McLaren, R. K. Grencis, Trichuris muris:
449 antigen recognition and transfer of immunity in mice by IgA monoclonal antibodies.
450 *Parasite Immunol* **13**, 1-12 (1991).
451 26. T. Gan, B. E. Li, B. P. Mishra, K. L. Jones, P. Ernst, MLL1 Promotes IL-7
452 Responsiveness and Survival during B Cell Differentiation. *J Immunol* **200**, 1682-1691
453 (2018).
454 27. M. Yamashita *et al.*, Crucial Role of MLL for the Maintenance of Memory T Helper Type
455 2 Cell Responses. *Immunity* **24**, 611-622 (2006).

456 28. N. Goveas *et al.*, MLL1 is required for maintenance of intestinal stem cells. *PLoS Genet*
457 **17**, e1009250 (2021).
458 29. M. Caganova *et al.*, Germinal center dysregulation by histone methyltransferase EZH2
459 promotes lymphomagenesis. *J Clin Invest* **123**, 5009-5022 (2013).
460 30. W. Béguelin *et al.*, EZH2 Is Required for Germinal Center Formation and Somatic EZH2
461 Mutations Promote Lymphoid Transformation. *Cancer cell* **23**, 677-692 (2013).
462 31. J. Zhang *et al.*, Disruption of KMT2D perturbs germinal center B cell development and
463 promotes lymphomagenesis. *Nat Med* **21**, 1190-1198 (2015).
464 32. K. Hatzi *et al.*, Histone demethylase LSD1 is required for germinal center formation and
465 BCL6-driven lymphomagenesis. *Nat Immunol* **20**, 86-96 (2019).
466 33. A. Di Pietro *et al.*, Targeting BMI-1 in B cells restores effective humoral immune
467 responses and controls chronic viral infection. *Nat Immunol* **23**, 86-98 (2022).
468 34. K. L. Good-Jacobson *et al.*, Regulation of germinal center responses and B-cell memory
469 by the chromatin modifier MOZ. *Proc Natl Acad Sci U S A* **111**, 9585-9590 (2014).
470 35. L. Kealy *et al.*, The Histone Methyltransferase DOT1L Is Essential for Humoral Immune
471 Responses. *Cell Rep* **33**, 108504 (2020).
472 36. Y. Nakata *et al.*, c-Myb, Menin, GATA-3, and MLL form a dynamic transcription
473 complex that plays a pivotal role in human T helper type 2 cell development. *Blood* **116**,
474 1280-1290 (2010).
475 37. A. Zaini *et al.*, Heterogeneous Tfh cell populations that develop during enteric helminth
476 infection predict the quality of type 2 protective response. *Mucosal Immunol* **16**, 642-657
477 (2023).

478 38. K. L. Good-Jacobson, Strength in diversity: Phenotypic, functional, and molecular
479 heterogeneity within the memory B cell repertoire. *Immunol Rev* **284**, 67-78 (2018).
480 39. K. J. Montaño, C. Cuéllar, J. Sotillo, Rodent Models for the Study of Soil-Transmitted
481 Helminths: A Proteomics Approach. *Front Cell Infect Microbiol* **11**, 639573 (2021).
482 40. N. M. Blackwell, K. J. Else, B cells and antibodies are required for resistance to the
483 parasitic gastrointestinal nematode Trichuris muris. *Infect Immun* **69**, 3860-3868 (2001).
484 41. A. Reboldi, J. G. Cyster, Peyer's patches: organizing B-cell responses at the intestinal
485 frontier. *Immunol Rev* **271**, 230-245 (2016).
486 42. O. Pabst *et al.*, Chemokine receptor CCR9 contributes to the localization of plasma cells
487 to the small intestine. *J Exp Med* **199**, 411-416 (2004).
488 43. K. S. Hayes, R. K. Grencis, Trichuris muris and comorbidities - within a mouse model
489 context. *Parasitology* **148**, 1-9 (2021).
490 44. N. Kamada *et al.*, Humoral Immunity in the Gut Selectively Targets Phenotypically
491 Virulent Attaching-and-Effacing Bacteria for Intraluminal Elimination. *Cell Host*
492 *Microbe* **17**, 617-627 (2015).
493 45. O. Pabst, E. Slack, IgA and the intestinal microbiota: the importance of being specific.
494 *Mucosal Immunol* **13**, 12-21 (2020).
495 46. C. Gutzeit, G. Magri, A. Cerutti, Intestinal IgA production and its role in host-microbe
496 interaction. *Immunol Rev* **260**, 76-85 (2014).
497 47. K. Llinas-Caballero, L. Caraballo, Helminths and Bacterial Microbiota: The Interactions
498 of Two of Humans' "Old Friends". *Int J Mol Sci* **23** (2022).
499 48. J. Kupritz, A. Angelova, T. B. Nutman, P. H. Gazzinelli-Guimaraes, Helminth-Induced
500 Human Gastrointestinal Dysbiosis: a Systematic Review and Meta-Analysis Reveals

501 Insights into Altered Taxon Diversity and Microbial Gradient Collapse. *mBio* **12**,
502 e0289021 (2021).
503 49. S. Z. Hasnain *et al.*, Mucin gene deficiency in mice impairs host resistance to an enteric
504 parasitic infection. *Gastroenterology* **138**, 1763-1771 (2010).
505 50. X. Liu *et al.*, Blautia-a new functional genus with potential probiotic properties? *Gut*
506 *Microbes* **13**, 1-21 (2021).
507 51. B. A. Rosa *et al.*, Whipworm-Associated Intestinal Microbiome Members Consistent
508 Across Both Human and Mouse Hosts. *Front Cell Infect Microbiol* **11**, 637570 (2021).
509 52. F. Zhang *et al.*, Curcumin Alleviates DSS-Induced Anxiety-Like Behaviors via the
510 Microbial-Brain-Gut Axis. *Oxid Med Cell Longev* **2022**, 6244757 (2022).
511 53. H. Wang *et al.*, Aberrant Gut Microbiome Contributes to Intestinal Oxidative Stress,
512 Barrier Dysfunction, Inflammation and Systemic Autoimmune Responses in MRL/lpr
513 Mice. *Front Immunol* **12**, 651191 (2021).
514 54. W. Y. Wu, P. L. Chou, J. C. Yang, C. T. Chien, Silicon-containing water intake confers
515 antioxidant effect, gastrointestinal protection, and gut microbiota modulation in the
516 rodents. *PloS one* **16**, e0248508 (2021).
517 55. L. Ma *et al.*, Spermidine improves gut barrier integrity and gut microbiota function in
518 diet-induced obese mice. *Gut Microbes* **12**, 1-19 (2020).
519 56. S. C. Lee *et al.*, Linking the effects of helminth infection, diet and the gut microbiota
520 with human whole-blood signatures. *PLoS Pathog* **15**, e1008066 (2019).
521 57. M. A. Toro-Londono, K. Bedoya-Urrego, G. M. Garcia-Montoya, A. L. Galvan-Diaz, J.
522 F. Alzate, Intestinal parasitic infection alters bacterial gut microbiota in children. *PeerJ* **7**,
523 e6200 (2019).

524 58. Y. Zhang, K. L. Good-Jacobson, Epigenetic regulation of B cell fate and function during
525 an immune response. *Immunol Rev* **288**, 75-84 (2019).
526 59. L. Cooper *et al.*, Type I interferons induce an epigenetically distinct memory B cell
527 subset in chronic viral infection. *Immunity* **57**, 1037-1055 (2024).
528 60. S. R. Park, E. K. Lee, B. C. Kim, P. H. Kim, p300 cooperates with Smad3/4 and Runx3 in
529 TGFbeta1-induced IgA isotype expression. *Eur J Immunol* **33**, 3386-3392 (2003).
530 61. A. Cerutti, The regulation of IgA class switching. *Nat Rev Immunol* **8**, 421-434 (2008).
531 62. A. Reboldi *et al.*, IgA production requires B cell interaction with subepithelial dendritic
532 cells in Peyer's patches. *Science* **352**, aaf4822 (2016).
533 63. P. Wang *et al.*, Global analysis of H3K4 methylation defines MLL family member targets
534 and points to a role for MLL1-mediated H3K4 methylation in the regulation of
535 transcriptional initiation by RNA polymerase II. *Mol Cell Biol* **29**, 6074-6085 (2009).
536 64. B. P. Mishra *et al.*, The histone methyltransferase activity of MLL1 is dispensable for
537 hematopoiesis and leukemogenesis. *Cell Rep* **7**, 1239-1247 (2014).
538 65. X. Huang *et al.*, Targeting Epigenetic Crosstalk as a Therapeutic Strategy for EZH2-
539 Aberrant Solid Tumors. *Cell* **175**, 186-199 e119 (2018).
540 66. J. E. Oh *et al.*, Intranasal priming induces local lung-resident B cell populations that
541 secrete protective mucosal antiviral IgA. *Sci Immunol* **6**, eabj5129 (2021).
542 67. T. R. Chern *et al.*, Discovery of Potent Small-Molecule Inhibitors of MLL
543 Methyltransferase. *ACS Med Chem Lett* **11**, 1348-1352 (2020).
544 68. K. Kwon *et al.*, Instructive role of the transcription factor E2A in early B lymphopoiesis
545 and germinal center B cell development. *Immunity* **28**, 751-762 (2008).

546 69. C. D. Jude *et al.*, Unique and independent roles for MLL in adult hematopoietic stem
547 cells and progenitors. *Cell Stem Cell* **1**, 324-337 (2007).
548 70. F. Antignano, S. C. Mullaly, K. Burrows, C. Zaph, Trichuris muris infection: a model of
549 type 2 immunity and inflammation in the gut. *J Vis Exp* 10.3791/2774 (2011).
550 71. K. J. Livak, T. D. Schmittgen, Analysis of relative gene expression data using real-time
551 quantitative PCR and the 2(-Delta Delta C(T)) Method. *Methods* **25**, 402-408 (2001).
552 72. K. A. Watt, D. H. Nussey, R. Maclellan, J. G. Pilkington, T. N. McNeilly, Fecal antibody
553 levels as a noninvasive method for measuring immunity to gastrointestinal nematodes in
554 ecological studies. *Ecol Evol* **6**, 56-67 (2016).
555 73. J. M. Smeekens *et al.*, Fecal IgA, Antigen Absorption, and Gut Microbiome Composition
556 Are Associated With Food Antigen Sensitization in Genetically Susceptible Mice. *Front*
557 *Immunol* **11**, 599637 (2020).
558 74. E. Bolyen *et al.*, Reproducible, interactive, scalable and extensible microbiome data
559 science using QIIME 2. *Nat Biotechnol* **37**, 852-857 (2019).
560 75. B. J. Callahan *et al.*, DADA2: High-resolution sample inference from Illumina amplicon
561 data. *Nat Methods* **13**, 581-583 (2016).
562 76. N. A. Bokulich *et al.*, q2-longitudinal: Longitudinal and Paired-Sample Analyses of
563 Microbiome Data. *mSystems* **3** (2018).
564 77. A. Dhariwal *et al.*, MicrobiomeAnalyst: a web-based tool for comprehensive statistical,
565 visual and meta-analysis of microbiome data. *Nucleic Acids Res* **45**, W180-W188 (2017).
566
567

568 **Figure Legends**

569 **Figure 1. MLL1 is required for GC B cell differentiation in Th2 cell-biased responses.**

570 (A and B) The expression of *Mll1* was assessed by RT-qPCR in B cell subsets sort-purified from
571 (A) the mesenteric lymph node (mLN) and (B) Peyer's patches of C57Bl/6 mice. (C) Follicular
572 (FO) B cells, GC B cells, PC and memory B cells were sort-purified from spleen and *Mll1*
573 expression assessed. FO B cells were sort-purified from C57Bl/6 mice, GC B cells were sort-
574 purified from C57Bl/6 mice immunized with NP-KLH in alum at d7 post-immunization, and
575 memory B cells and PC were sort-purified from C57Bl/6 mice immunized with NP-KLH in alum
576 at d28 post-immunization. Expression of *Mll1* was normalized to *Rpl32* and then normalized to
577 naïve (A, B) or follicular (C) B cells. (D) Schematic depiction of *T. muris* experimental setup. (E)
578 Flow cytometric analyses of $B220^{+}IgD^{lo}CD95^{hi}CD38^{lo}$ (GC B cells) in mLN *T. muris*-infected
579 $Cd23^{cre/+}$ and $Mll1^{f/f}Cd23^{cre/+}$ mice at d14 and d28 post-infection. The number in plots shows the
580 frequency of GC B cells within the $B220^{+}IgD^{lo}$ population. (F and G) Frequency (F) and number
581 (G) of GC B cells post-infection. Data are combined from three independent experiments per time
582 point; n=9 (d14), n=7-9 (d28) and n=10-11 (d35) per genotype. (H) Representative histological
583 images of mLN from d14 *T. muris*-infected $Cd23^{cre/+}$ and $Mll1^{f/f}Cd23^{cre/+}$ mice: B220 (red) and
584 PNA (blue). Scale bar = 100μM (I) Flow cytometric analysis of NP^{+} GC B cells
585 ($B220^{+}IgD^{lo}CD95^{hi}NP^{+}$) from d14 post-immunized $Cd23^{cre/+}$ and $Mll1^{f/f}Cd23^{cre/+}$ mice. (J and K)
586 Frequency (J) and number (K) of GC B cells post-immunization at d14 and d28. Data are combined
587 from two independent experiments per time point; n=7 (d14) and n=3-6 (d28) per genotype. Error
588 bars indicate mean ± SEM, *$p < 0.05$, **$p < 0.01$, ***$p < 0.001$, Mann-Whitney test.

589

590 **Figure 2. B cell-intrinsic MLL1 deletion leads to rapid worm clearance and increased IgA.**
591 (A) Number of worms in the caecum from *T. muris*-infected *Cd23*$^{cre/+}$ and *Mll1*$^{f/f}$*Cd23*$^{cre/+}$ mice at
592 d14, d28 and d35 post-infection. Data are combined from 2-3 experiments per time point; n=10
593 (d14); n=7-9 (d28); n=7-8 (d35) per genotype. (B) *T. muris*-specific serum IgG1 at d14 post-
594 infection. (C) Representative flow cytometric plots of IgG1^{+}GC B cells (IgG1^{+}CD95^{hi}CD38^{lo}) and
595 IgE^{+} GC B cells (IgE^{+}CD95^{hi}CD38^{lo}) in mLN at d14. The number in plots shows the frequency of
596 IgG1^{+} or IgE^{+} within the GC B cell population. (D-E) Frequency of (D) IgG1^{+} GC B cells and (E)
597 IgG1^{+} PC (IgG1^{+}B220^{lo}CD138^{hi}). Data are combined from three independent experiments, n=9
598 per genotype. (F-G) Frequency of (F) IgE^{+} GC B cells and (G) IgE^{+} PC (IgE^{+}B220^{lo}CD138^{hi}). Data
599 are combined from two independent experiments, n=6 per genotype. (H) Representative plots
600 shown of IgA^{+} GC B cells (IgA^{+}CD95^{hi}CD38^{lo}) in mLN or Peyer's patches at d14. The number in
601 plots shows the frequency of IgA^{+} within the GC B cell population. (I and J) Frequency of IgA^{+}
602 GC B cells in the (I) mLN and (J) Peyer's Patches (PP). Data are combined from two independent
603 experiments. n=8 or 9 per genotype. (K) Serum IgA and (L) fecal IgA from d14 *T. muris*-infected
604 *Cd23*$^{cre/+}$ and *Mll1*$^{f/f}$*Cd23*$^{cre/+}$ mice. Data are combined from 3-4 independent experiments, n=12
605 per genotype. Error bars indicate mean ± SEM. *$p < 0.05$, **$p < 0.01$, Mann-Whitney test. (M-O)
606 B cells were stimulated in culture with CD40L, IL-4, IL-5, TGFβ and retinoic acid for 4 days. (M)
607 Frequency of B cells, (N) frequency of PC, (O) total number of IgA^{+} PC, and (P) IgA in supernatant
608 at d4 post-stimulation. Data are combined from two individual experiments, n=5 per genotype.
609 Error bars indicate mean +- SEM, *$p < 0.05$, **$p < 0.01$, Mann-Whitney test.
610

611 **Figure 3. MLL1 regulates the expression of genes related to IgA production.**

612 (A) Heatmap of RNA-sequencing data with fold change >2 and q-value (FDR-adjusted p-value) <
613 0.05; each column is an independent sample obtained from sort-purified GC B cells
614 ($B220^{+}IgD^{lo}CD95^{hi}CD38^{lo}$) from mLN of d13 *T.muris*-infected $Cd23^{cre/+}$ and $Mll1^{f/f}Cd23^{cre/+}$ mice,
615 n=2 per genotype. (B) KEGG enrichment pathway analysis of differential gene expression. The
616 size of the dot is positively correlated with the number of differential genes in the pathway. (C)
617 Plots showing FPKM (Fragments per kilo base of transcript per million mapped fragments) for
618 *Ccr9*. (D) Representative flow cytometric plots of $CCR9^{+}IgA^{+}$ PC ($CCR9^{+}IgA^{+}B220^{lo}CD138^{hi}$) in
619 mLN from d14 *T. muris*-infected $Cd23^{cre/+}$ and $Mll1^{f/f}Cd23^{cre/+}$ mice. (E) CCR9 geometric mean
620 fluorescence intensity (MFI) and $CCR9^{+}$ frequency within IgA^{+} PC in mLN; n=4 per genotype.
621 (F) Representative plots of $CCR9^{+}IgA^{+}$ PC ($CCR9^{+}IgA^{+}CD3^{-}B220^{lo}Blimp1^{+}$) in colon lamina
622 propria from d14 *T. muris*-infected $Cd23^{cre/+}$ and $Mll1^{f/f}Cd23^{cre/+}$ mice. (G) Frequency of $CCR9^{+}$
623 cells in IgA^{+} PC population in colon lamina propria. Data shown are from 2 experiments, n=6 per
624 genotype. Error bars indicate mean ± SEM. *p < 0.05, Mann-Whitney test. (H) $Mll1^{f/f}$ and
625 $Mll1^{f/f}Cd23^{cre/+}$ mice were infected with *C. rodentium* and assessed at d14 post-infection. (I)
626 Frequency of $CCR9^{+}IgA^{+}$ PC in mLN. (J) Frequency of $CCR9^{+}$ PC and $CCR9^{+}IgA^{+}$ B cells in
627 colon lamina propria. *p < 0.05, unpaired t-test. (K) Serum IgA, combined from two independent
628 experiments. *p < 0.05, Mann-Whitney test.

629

630 **Figure 4. B cell-specific MLL1 deletion induces a shift in microbiota.**

631 (A) Representative images from histological analyses of swiss-rolled cecum tissue from d14 *T.*
632 *muris*-infected $Cd23^{cre/+}$ and $Mll1^{f/f}Cd23^{cre/+}$ mice. (B) The number of goblet cells per crypt was
633 measured for 20 crypts per mouse across the entire length of the cecum. Combined data from two

634 independent experiments, n=8 per genotype. Error bars indicate mean ± SEM. *p < 0.05, Mann-
635 Whitney test. (C) Schematic depiction of *T. muris* experimental setup to assess microbiome. (D)
636 Microbiota at genus level in cecum feces from d14 *T. muris*-infected *Cd23*$^{cre/+}$ and *Mll1*$^{f/f}$*Cd23*$^{cre/+}$
637 mice was assessed by 16S rRNA gene sequencing. Linear Discriminant Analysis Effect Size
638 (LefSe) analysis with Log LDA score above 2.0 and P-value cutoff 0.05; n= 5 per genotype. (E)
639 The log transformed counts (abundance) of significantly changed bacteria identified by
640 MetagenomeSeq analysis (adjusted p-value cutoff of 0.05).
641
642 **Supplemental Figure Legend**
643 **Supplemental Figure S1.**
644 (A) Fecal IgA and (B) serum IgA from uninfected *Cd23*$^{cre/+}$ and *Mll1*$^{f/f}$*Cd23*$^{cre/+}$ mice. n= 6 per
645 genotype. (C) Microbiota at genus level in cecum feces from d14 *T. muris*-infected *Cd23*$^{cre/+}$ and
646 *Mll1*$^{f/f}$*Cd23*$^{cre/+}$ mice was assessed by 16S rRNA gene sequencing. β-diversity profiling of 16s
647 sequencing. (D) The relative abundance of microbiota at genus level in caecum feces from *T.*
648 *muris*-infected *Cd23*$^{cre/+}$ and *Mll1*$^{f/f}$*Cd23*$^{cre/+}$ mice on d14 post-infection by 16S rRNA gene
649 sequencing. n= 5 per genotype.
650
651

FIGURE 1

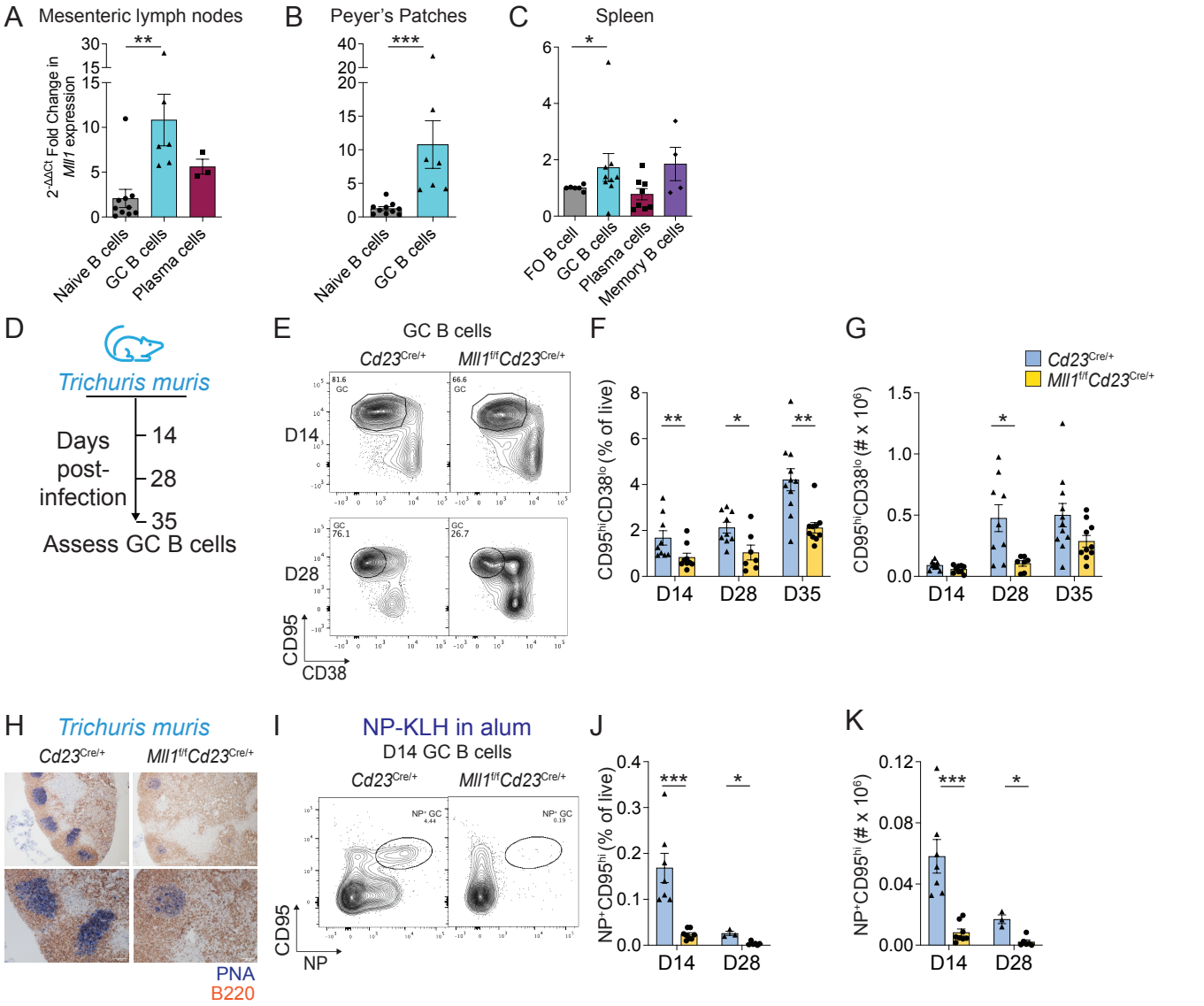
A
Mesenteric lymph nodes
2-ΔΔCt Fold Change in Mll1 expression
Naive B cells
GC B cells
Plasma cells
B
Peyer's Patches
C
Spleen
FO B cell
Memory B cells
D
Trichuris muris
Days post-infection
14
28
35
Assess GC B cells
E
GC B cells
Cd23Cre/+
Mll1f/fCd23Cre/+
D14
D28
CD95
CD38
F
CD95hiCD38lo (% of live)
D14
D28
D35
G
CD95hiCD38lo (# x 10^6)
H
Trichuris muris
PNA
B220
I
NP-KLH in alum
D14 GC B cells
NP
J
NP+CD95hi (% of live)
K
NP+CD95hi (# x 10^6)

FIGURE 2

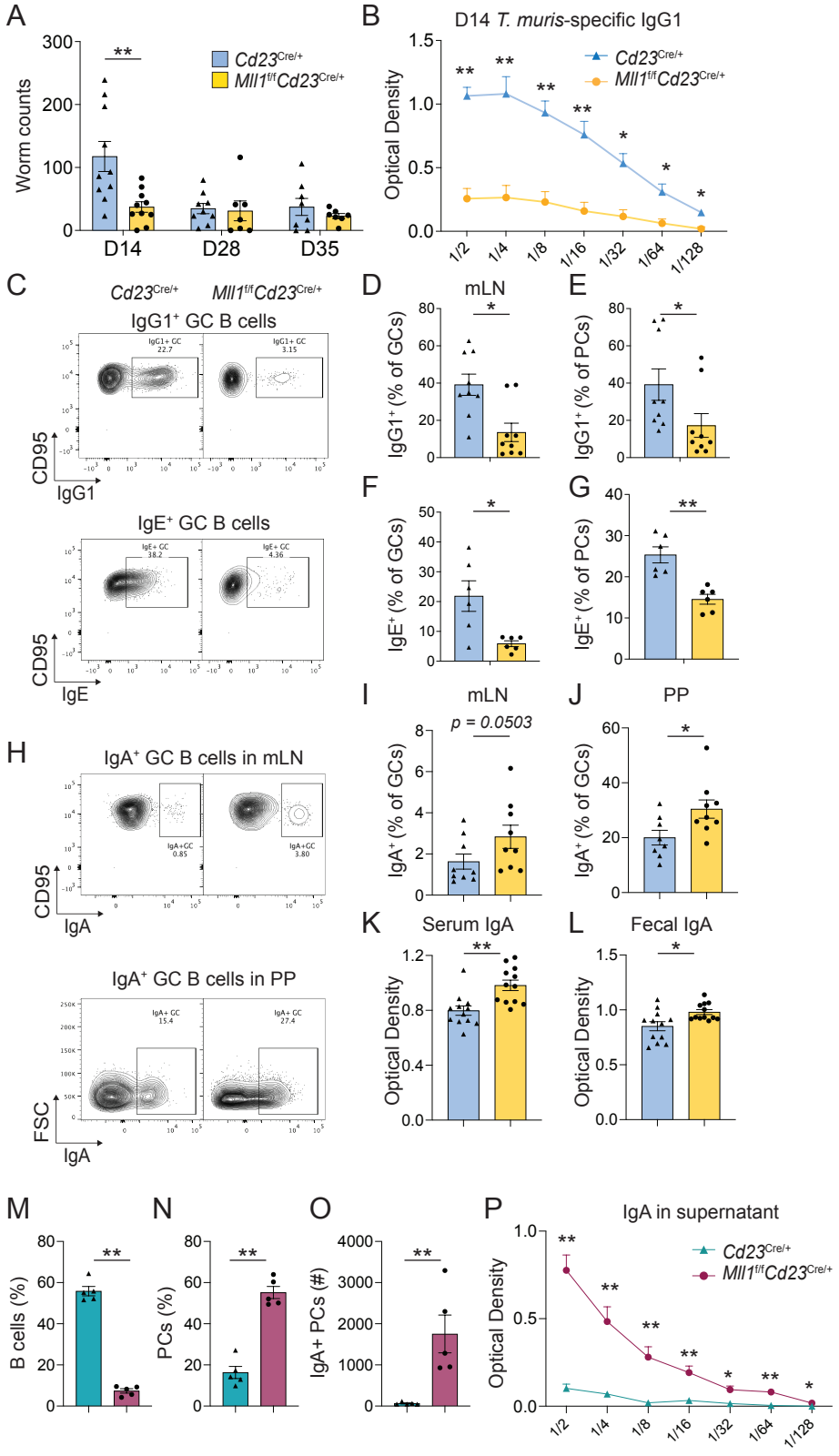
A
Worm counts
Cd23Cre/+
Mll1f/fCd23Cre/+
D14
D28
D35
B
D14 T. muris-specific IgG1
Optical Density
1/2
1/4
1/8
1/16
1/32
1/64
1/128
C
Cd23Cre/+
Mll1f/fCd23Cre/+
IgG1+ GC B cells
CD95
IgG1
IgE+ GC B cells
IgE
D
mLN
IgG1+ (% of GCs)
E
IgG1+ (% of PCs)
F
IgE+ (% of GCs)
G
IgE+ (% of PCs)
H
IgA+ GC B cells in mLN
IgA
IgA+ GC B cells in PP
FSC
I
mLN
p = 0.0503
IgA+ (% of GCs)
J
PP
IgA+ (% of GCs)
K
Serum IgA
Optical Density
L
Fecal IgA
Optical Density
M
B cells (%)
N
PCs (%)
O
IgA+ PCs (#)
P
IgA in supernatant
Optical Density
Cd23Cre/+
Mll1f/fCd23Cre/+

FIGURE 3

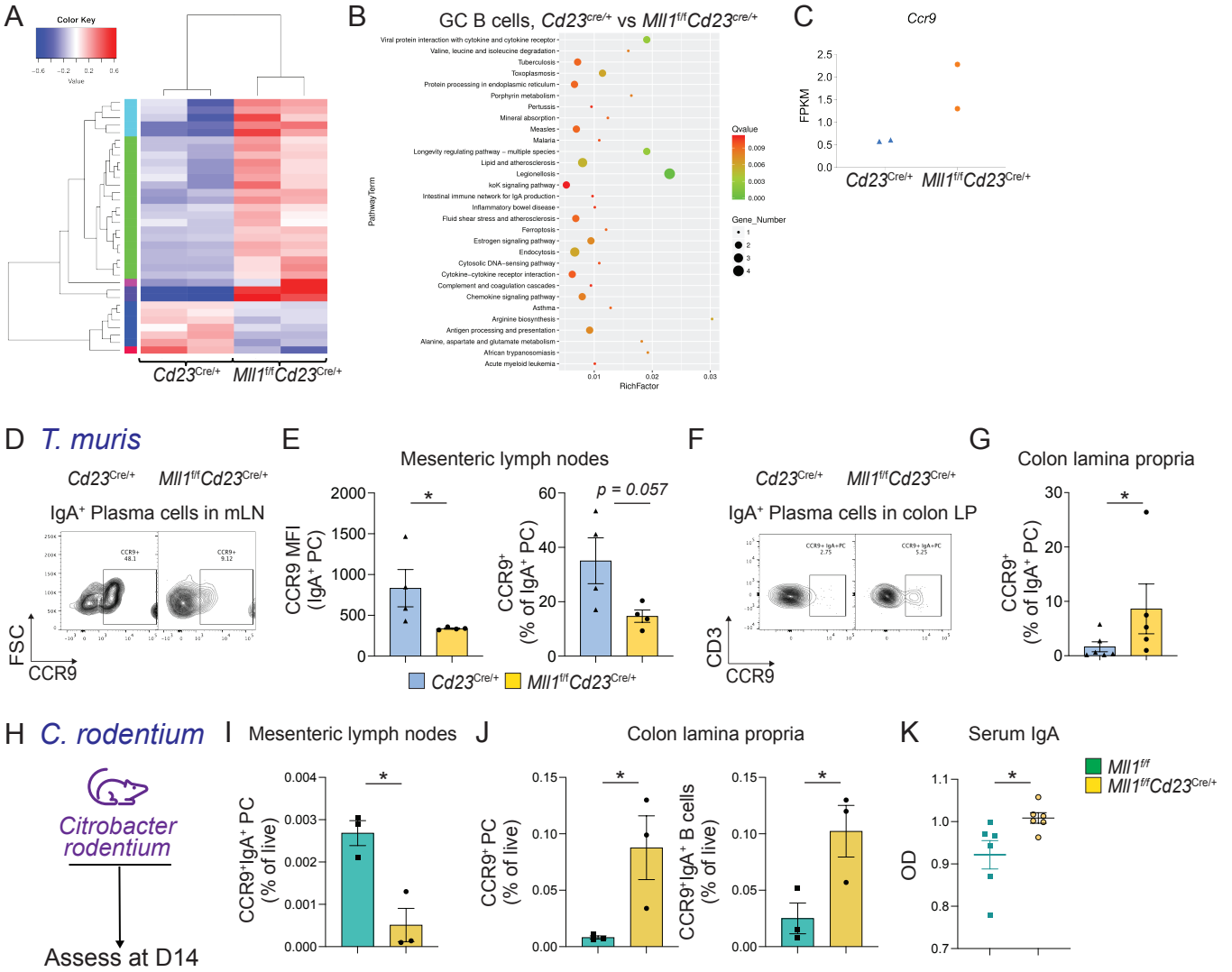
A
Color Key
Value
Cd23Cre/+
Mll1f/fCd23Cre/+
B
GC B cells, Cd23cre/+ vs Mll1f/fCd23cre/+
Viral protein interaction with cytokine and cytokine receptor
Valine, leucine and isoleucine degradation
Tuberculosis
Toxoplasmosis
Protein processing in endoplasmic reticulum
Porphyrin metabolism
Pertussis
Mineral absorption
Measles
Malaria
Longevity regulating pathway – multiple species
Lipid and atherosclerosis
Legionellosis
koK signaling pathway
Intestinal immune network for IgA production
Inflammatory bowel disease
Fluid shear stress and atherosclerosis
Ferroptosis
Estrogen signaling pathway
Endocytosis
Cytosolic DNA–sensing pathway
Cytokine–cytokine receptor interaction
Complement and coagulation cascades
Chemokine signaling pathway
Asthma
Arginine biosynthesis
Antigen processing and presentation
Alanine, aspartate and glutamate metabolism
African trypanosomiasis
Acute myeloid leukemia
Pathway/Term
RichFactor
Qvalue
Gene_Number
C
Ccr9
FPKM
Cd23Cre/+
Mll1f/fCd23Cre/+
D T. muris
Cd23Cre/+
Mll1f/fCd23Cre/+
IgA+ Plasma cells in mLN
FSC
CCR9
E
Mesenteric lymph nodes
CCR9 MFI (IgA+ PC)
CCR9+ (% of IgA+ PC)
p = 0.057
Cd23Cre/+
Mll1f/fCd23Cre/+
F
Cd23Cre/+
Mll1f/fCd23Cre/+
IgA+ Plasma cells in colon LP
CD3
CCR9
G
Colon lamina propria
CCR9+ (% of IgA+ PC)
H C. rodentium
Citrobacter rodentium
Assess at D14
I Mesenteric lymph nodes
CCR9+IgA+ PC (% of live)
J
Colon lamina propria
CCR9+ PC (% of live)
CCR9+IgA+ B cells (% of live)
K
Serum IgA
OD
Mll1f/f
Mll1f/fCd23Cre/+

FIGURE 4

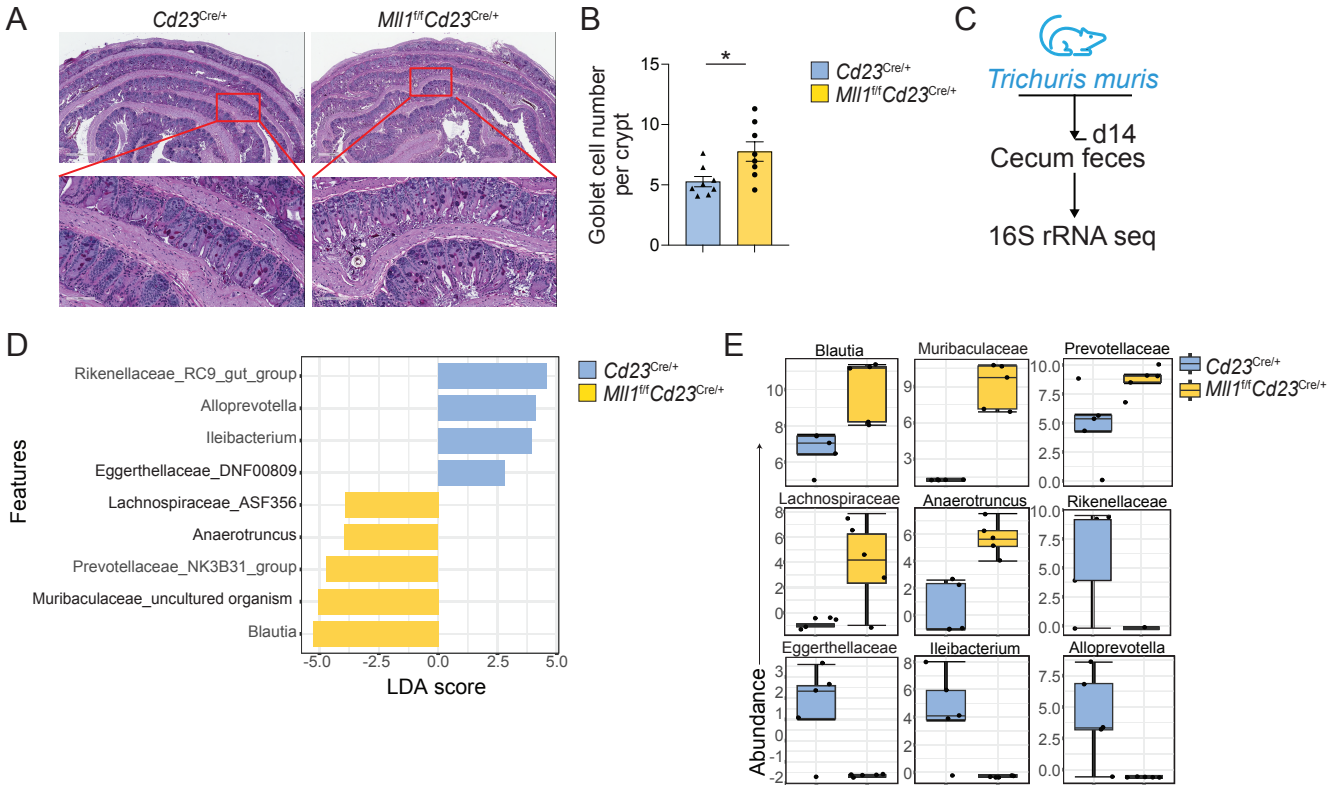
A
Cd23Cre/+
Mll1f/fCd23Cre/+
B
Goblet cell number per crypt
15
10
5
0
*
Cd23Cre/+
Mll1f/fCd23Cre/+
C
Trichuris muris
d14
Cecum feces
16S rRNA seq
D
Features
Rikenellaceae_RC9_gut_group
Alloprevotella
Ileibacterium
Eggerthellaceae_DNF00809
Lachnospiraceae_ASF356
Anaerotruncus
Prevotellaceae_NK3B31_group
Muribaculaceae_uncultured organism
Blautia
-5.0
-2.5
0.0
2.5
5.0
LDA score
Cd23Cre/+
Mll1f/fCd23Cre/+
E
Abundance
Blautia
Muribaculaceae
Prevotellaceae
Lachnospiraceae
Anaerotruncus
Rikenellaceae
Eggerthellaceae
Ileibacterium
Alloprevotella
Cd23Cre/+
Mll1f/fCd23Cre/+

FIGURE S1

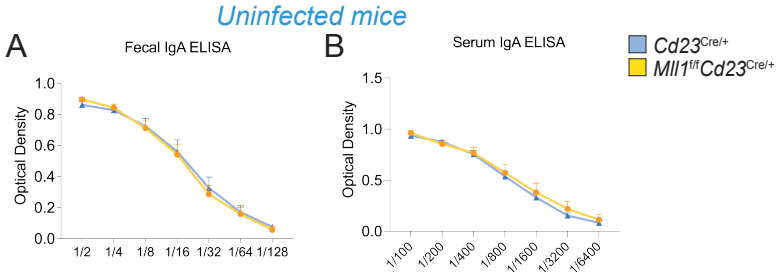
Uninfected mice
A
Fecal IgA ELISA
Optical Density
1.0
0.8
0.6
0.4
0.2
0.0
1/2
1/4
1/8
1/16
1/32
1/64
1/128
B
Serum IgA ELISA
Optical Density
1.5
1.0
0.5
0.0
1/100
1/200
1/400
1/800
1/1600
1/3200
1/6400
Cd23Cre/+
Mll1f/fCd23Cre/+

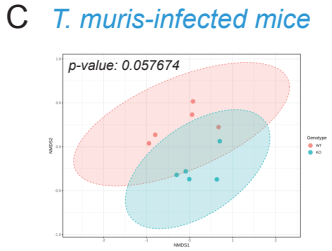
C
T. muris-infected mice
p-value: 0.057674

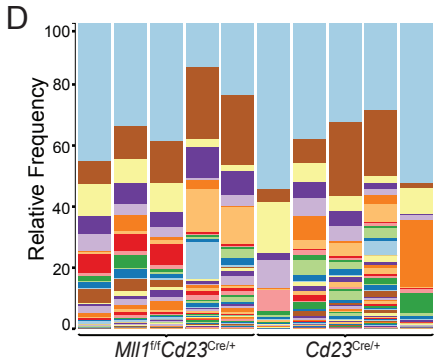
D
Relative Frequency
100
80
60
40
20
0
Mll1f/fCd23Cre/+
Cd23Cre/+